PP + PS = SS

Vladimir Grechka* and Ilya Tsvankin[‡]

ABSTRACT

Converted (PS) waves can provide important information about shear-wave velocity and, in the presence of anisotropy, about the medium parameters responsible for both P- and S-wave propagation. Kinematics and amplitudes of reflected PS-waves, however, possess such undesirable features as moveout asymmetry, reflection point dispersal, and polarity reversal, which preclude application of conventional velocity-analysis methods to mode conversions.

Rather than using PS-wave kinematics directly, here we propose a method for reconstructing SS-wave reflection traveltimes from PP and PS data. The required preprocessing steps include picking of PP and PS traveltimes on prestack data and identification (correlation) of the PP and PS events from the same interfaces. The key idea of the method is to match the reflection slopes (horizontal slownesses) on common-receiver PP and PS gathers. This procedure allows us to find the coordinates of receivers that record PP- and PS-waves reflected at exactly the same (albeit unknown) subsurface points and to determine the shear-wave reflection traveltime t_{SS} as a simple combination of the PP and PS traveltimes. The reconstructed SS-wave moveout can then be processed by velocity-analysis methods designed for pure reflection modes. The developed technique, however, cannot be used to compute the true amplitudes of the reflected SS-waves.

Our method has the following attractive features:

1) No information about the velocity field or anisotropic parameters is required to obtain SS-wave traveltimes from PP and PS data. If the input PP and PS arrivals are picked correctly and correspond to the same reflector, the method produces exact traveltimes t_{SS}.

2) The estimates of traveltimes and reflection slopes are local, which makes reflection-point dispersal irrelevant.

3) Another consequence of the local nature of this procedure is that the portion of PS data in the vicinity of the polarity reversal (where the PS amplitudes are small) can be muted out without compromising the quality of t_{SS} estimates for source–receiver pairs with high PS amplitudes.

INTRODUCTION

Because of the high cost of shear-wave excitation, the difficulty of placing sources on the sea floor, and the often poor quality of SS-wave data, it has become a practice in seismic imaging and parameter estimation to replace pure SS reflections with mode-converted PS-waves. Converted waves are of particular importance in offshore seismic, where they represent the only available type of shear energy. For a number of exploration scenarios, PS-waves provide valuable information about the subsurface structure or medium properties that cannot be inferred from conventional PP-wave data. Examples include imaging through gas chimneys, characterization of naturally fractured reservoirs, and estimation of rock and fluid parameters (e.g., Granli et al., 1999; Pérez et al., 1999; Thomsen, 1999; Gaiser, 2000).

In anisotropic media, shear-wave data play a crucial role in velocity analysis and parameter estimation because PP-wave reflection traveltimes alone usually are insufficient for estimating even the subset of medium parameters responsible for P-wave propagation. For example, if the medium is transversely isotropic with a vertical symmetry axis (VTI), reflection moveout of PP-waves generally constrains just two parameter combinations: the NMO velocity for a horizontal reflector $V_{\mathrm{nmo},P}(0)$

and the anellipticity parameter η (Alkhalifah and Tsvankin, 1995; Grechka and Tsvankin, 1998). [It is possible to invert PP reflection traveltimes for the vertical velocity V_{P0} and Thomsen anisotropic coefficients ϵ and δ only for some VTI models with laterally heterogeneous overburden (Grechka, Pech, and Tsvankin, 2000a,b).] The addition of PS (PSV) reflection traveltimes to PP moveout in VTI media helps to resolve the vertical P- and S-wave velocities and the parameters ϵ and δ, provided the reflector has a mild dip and the data are acquired for a wide range of azimuths (Tsvankin and Grechka, 2000a,b). Joint inversion of PP and PS data can be used to estimate the parameters of the more complicated orthorhombic and monoclinic media as well (Grechka et al., 1999; Grechka, Contreras, and Tsvankin, 2000).

However, parameter-estimation algorithms operating with PS data are impeded by several inherent features of reflection moveout of mode-converted waves. The most significant problem in PS-wave velocity analysis stems from the asymmetry of PS moveout with respect to zero offset, both on common-midpoint (CMP) and common-conversion-point (CCP) gathers (see examples in Tsvankin and Grechka, 2000a,b). In contrast, for pure modes (PP or SS) reflection traveltime t between the source located at $\mathbf{x}^{(1)}$ and the receiver at $\mathbf{x}^{(2)}$ remains the same if the source and receiver positions are interchanged:

$$t_{PP}\big(\mathbf{x}^{(1)}, \mathbf{x}^{(2)}\big) = t_{PP}\big(\mathbf{x}^{(2)}, \mathbf{x}^{(1)}\big)$$

and

$$t_{SS}\big(\mathbf{x}^{(1)}, \mathbf{x}^{(2)}\big) = t_{SS}\big(\mathbf{x}^{(2)}, \mathbf{x}^{(1)}\big). \qquad (1)$$

Hence, moveout of pure-mode reflections on CMP gathers is an even function of the source–receiver offset x and can be described by the traveltime series $t^2(x^2)$. The hyperbolic moveout equation, routinely applied in seismic processing, is a truncated form of this series used for moderate offsets not exceeding reflector depth.

Converted-wave traveltimes are symmetric with respect to zero offset only if the subsurface is composed of laterally homogeneous horizontal layers with a horizontal symmetry plane. Various aspects of PS-wave kinematics in this special case are discussed for isotropic media by Tessmer and Behle (1988) and for anisotropic media by Seriff and Sriram (1991), Tsvankin and Thomsen (1994), Grechka et al. (1999), Thomsen (1999), and others.

In general, however, the PS-wave reflection traveltime $t_{PS}(\mathbf{x}^{(1)}, \mathbf{x}^{(2)})$ is not reciprocal with respect to the source and receiver positions:

$$t_{PS}\big(\mathbf{x}^{(1)}, \mathbf{x}^{(2)}\big) \neq t_{PS}\big(\mathbf{x}^{(2)}, \mathbf{x}^{(1)}\big). \qquad (2)$$

The asymmetry of PS moveout makes the series $t^2(x^2)$ in general, and the hyperbolic moveout equation in particular, invalid for mode conversions. For instance, moveout (stacking) velocity of PS-waves generally takes two different values for positive and negative offsets on a CMP gather; Thomsen (1999) calls this phenomenon the diodic velocity. Therefore, efficient velocity-analysis methods developed for pure modes, such as algorithms for anisotropic stacking-velocity tomography (Grechka, Pech and Tsvankin, 2000a,b), cannot be applied to PS-waves.

Tsvankin and Grechka (2000b) have attempted to remove the moveout asymmetry by resorting the data into the so-called RTM (resorting to traveltime minimum) gathers wherein the moveout is locally symmetric in the vicinity of the traveltime minimum. Their procedure, however, does not remove the reflection point dispersal, requires building different gathers for each source–receiver pair, and leads to complicated expressions for the NMO velocity in RTM geometry.

Here, we suggest abandoning the whole concept of PS-wave moveout analysis. Instead, we use PP- and PS-wave reflection traveltimes t_{PP} and t_{PS} to compute the SS-wave traveltimes t_{SS} for the same reflector; this explains the title "PP + PS = SS" of our paper. We reconstruct t_{SS} by obtaining information about the PP and PS reflection slopes, or horizontal slownesses, from the common-receiver gathers. Matching the slopes helps to identify the receivers that record PP and SS events reflected from exactly the same subsurface points and helps to find the traveltime t_{SS} as a simple linear combination of the recorded times t_{PP} and t_{PS}. We begin by describing the concept of the method in two dimensions and then discuss its extension to three dimensions. Finally, a test on ray-traced synthetic data illustrates application of the method in practice.

ANALYTIC FORMULATION

2-D problem

Suppose PP- and PS-wave reflection data are acquired along a straight line in the dip direction of the subsurface structure and, if the medium is anisotropic, the vertical incidence plane is a plane of symmetry. Then the reflected rays do not deviate from the incidence plane, and reflection traveltime depends on only the in-plane velocity field (i.e., the kinematic problem is two dimensional). For the purpose of theoretical development, it is assumed that the P-wave sources and two-component receivers are continuously distributed along the line. The receivers record both PP reflections and P-to-S conversions at the reflector; hence, using the terminology of Thomsen (1999), we treat only C-waves rather than conversions at intermediate interfaces. The most fundamental assumption made here is that both PP- and PS-waves are reflected from the same boundary in the subsurface. (Errors arising from violating this assumption will be discussed later.) The velocity field in our model can be arbitrary and will not be specified throughout this paper.

The goal of our procedure is to identify the PP and PS rays excited by the same source and reflected at the same point on the interface. Let us examine PP data resorted into the common-receiver gather for a particular receiver located at $x^{(2)}$ (Figure 1). The reflection traveltime $t_{PP}(x^{(1)}, x^{(2)})$ in the vicinity of the source at $x^{(1)}$ can be approximated by a linear function of the source coordinate $x^{(1)}$. Tracking the PP reflection event on the common-receiver gather, we can find its traveltime $t_{PP}(x^{(1)}, x^{(2)})$, along with the local slope

$$p_{PP}\big(x^{(1)}, x^{(2)}\big) = \left. \frac{dt_{PP}\big(x, x^{(2)}\big)}{dx} \right|_{x=x^{(1)}}. \qquad (3)$$

It is known from ray theory that the slope $p_{PP}(x^{(1)}, x^{(2)})$ is equal to the horizontal in-line component of the slowness vector (measured at the source location) of the ray that travels from the source $x^{(1)}$ to the receiver $x^{(2)}$. [The parameter $p_{PP}(x^{(1)}, x^{(2)})$ is conventionally called the ray parameter; it can also be called the inverse of the profile or apparent velocity on

the common-receiver gather.] This ray satisfies Snell's law at the (generally unknown from surface data) reflection point R (Figure 1), which means that

$$\left[\mathbf{p}^P\left(x^{(1)} \to R\right) - \mathbf{p}^P\left(R \to x^{(2)}\right)\right] \times \mathbf{b}(R) = 0. \qquad (4)$$

Here $\mathbf{p}^P(x^{(1)} \to R)$ and $\mathbf{p}^P(R \to x^{(2)})$ are the slowness vectors of the downgoing and upgoing P rays, respectively, and $\mathbf{b}(R)$ is the normal to the reflector. All quantities in equation (4) are evaluated at the reflection point R, where the projections of the slowness vectors $\mathbf{p}^P(x^{(1)} \to R)$ and $\mathbf{p}^P(R \to x^{(2)})$ onto the reflector should be equal to each other.

Next, we examine a PS-wave converted from P to S at the same reflector (Figure 2). Again, we resort the data into common-receiver gathers for different receiver positions $x^{(3)}$ to obtain the traveltimes $t_{PS}(x^{(1)}, x^{(3)})$ and the local reflection slopes at the source position $x^{(1)}$,

$$p_{PS}\left(x^{(1)}, x^{(3)}\right) = \left. \frac{dt_{PS}\left(x, x^{(3)}\right)}{dx} \right|_{x=x^{(1)}}. \qquad (5)$$

We are interested in finding a specific receiver location $x^{(3)}$, such that

$$p_{PP}\left(x^{(1)}, x^{(2)}\right) = p_{PS}\left(x^{(1)}, x^{(3)}\right). \qquad (6)$$

Equation (6) can be solved for the unknown coordinate

$$x^{(3)} \equiv x^{(3)}\left(x^{(1)}, x^{(2)}\right) \qquad (7)$$

by scanning over receiver locations $x^{(3)}$ along the line. It is not clear in advance whether such a solution exists for any given coordinates $x^{(1)}$ and $x^{(2)}$ and whether it is unique. If it does not exist (see the numerical example below), the whole procedure is simply repeated for another pair of $(x^{(1)}, x^{(2)})$. If equation (6) has several solutions, as in the case of shear-wave triplications
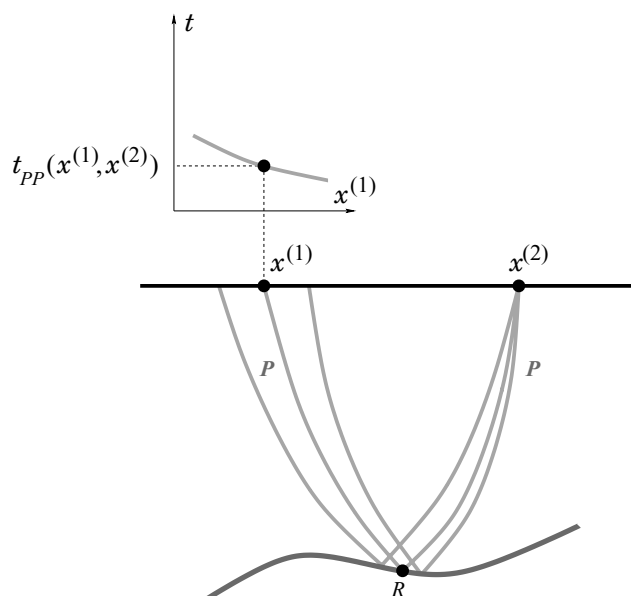
(cusps), it is possible to find all of them and reconstruct the multivalued traveltime t_{SS}.

Suppose equation (6) has at least one solution $x^{(3)}$. Then rays $x^{(1)}Rx^{(2)}$ and $x^{(1)}Rx^{(3)}$ in Figure 2 have a common segment $x^{(1)}R$ and, therefore, the same reflection point R. Indeed, both rays are excited at the same source $x^{(1)}$ and in the same direction specified by the horizontal slowness $p_{PP}(x^{(1)}, x^{(2)}) = p_{PS}(x^{(1)}, x^{(3)})$ [see equation (6)]. Since the initial conditions for those two rays are identical and the rays travel through the same medium, their trajectories have to coincide between the source and the reflection point R, where one of the downgoing waves gets converted into an S-wave.

An important point to mention is that the slowness vector of the incident P ray just before the conversion is equal to $\mathbf{p}^P(x^{(1)} \to R)$, the quantity that appears in Snell's law (4) for the pure PP-wave reflection. The reflected PS ray $x^{(1)}Rx^{(3)}$ also obeys Snell's law,

$$\left[\mathbf{p}^P\left(x^{(1)} \to R\right) - \mathbf{p}^S\left(R \to x^{(3)}\right)\right] \times \mathbf{b}(R) = 0, \qquad (8)$$

where $\mathbf{p}^S(R \to x^{(3)})$ is the slowness vector of the upgoing S ray at the reflection point R.

Next, let us switch the source and receiver positions by placing the source at $x^{(2)}$ and the receiver at $x^{(1)}$. Repeating the same event-tracking procedure on the common-receiver PP-wave gather yields the reflection slope (Figure 3)

$$p_{PP}\left(x^{(2)}, x^{(1)}\right) = \left. \frac{dt_{PP}\left(x, x^{(1)}\right)}{dx} \right|_{x=x^{(2)}}. \qquad (9)$$

Note that although the traveltimes $t_{PP}(\mathbf{x}^{(1)}, \mathbf{x}^{(2)})$ and $t_{PP}(\mathbf{x}^{(2)}, \mathbf{x}^{(1)})$ coincide with each other [equation (1)], the

FIG. 1. Reflected PP rays and traveltimes recorded on a common-receiver gather.
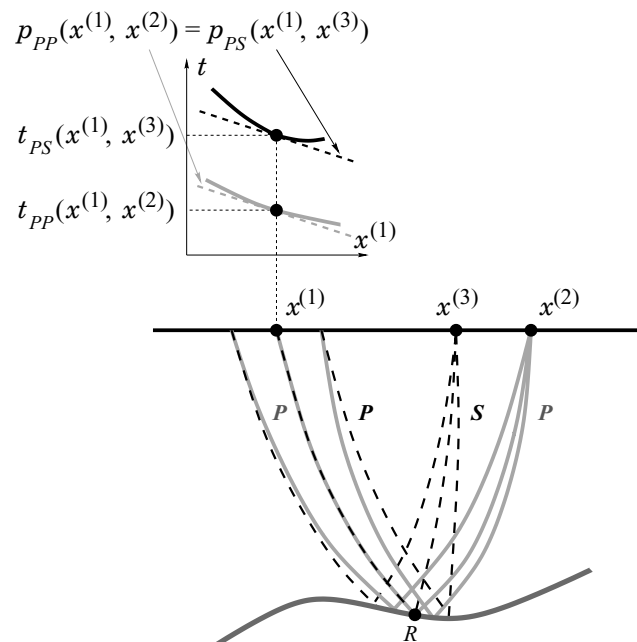

FIG. 2. The reflection slope $p_{PS}(x^{(1)}, x^{(3)})$ on the common-receiver gather for the PS-wave recorded at $x^{(3)}$ is equal to the slope $p_{PP}(x^{(1)}, x^{(2)})$ on the PP-wave common-receiver gather at $x^{(2)}$.

corresponding slopes are generally different, unless the medium is laterally homogeneous:

$$p_{PP}\left(x^{(1)}, x^{(2)}\right) \neq p_{PP}\left(x^{(2)}, x^{(1)}\right). \quad (10)$$

Repeating the procedure described above, we find the receiver coordinate $x^{(4)}$ for which the slope $p_{PS}(x^{(2)}, x^{(4)})$ of the converted PS-wave on the common-receiver gather satisfies the condition

$$p_{PP}\left(x^{(2)}, x^{(1)}\right) = p_{PS}\left(x^{(2)}, x^{(4)}\right). \quad (11)$$

The PS-wave traveltime for this source–receiver pair is $t_{PS}(x^{(2)}, x^{(4)})$. Hence, the converted-wave ray $x^{(2)}Rx^{(4)}$ in Figure 3 has the same reflection point R as that of the two previously computed rays. The slowness vectors of the downgoing P and upgoing S rays for the path $x^{(2)}Rx^{(4)}$ obey Snell's law at R:

$$\left[\mathbf{p}^{P}\left(x^{(2)} \to R\right) - \mathbf{p}^{S}\left(R \to x^{(4)}\right)\right] \times \mathbf{b}(R) = 0. \quad (12)$$

Thus, we have identified three ray trajectories [$x^{(1)}Rx^{(2)}$, $x^{(1)}Rx^{(3)}$, and $x^{(2)}Rx^{(4)}$] with the same reflection point R (Figure 3). Combining the segments $Rx^{(3)}$ and $Rx^{(4)}$ yields a pure shear ray $x^{(3)}Rx^{(4)}$.

Next, it has to be proven that the trajectory $x^{(3)}Rx^{(4)}$ corresponds to a real reflected SS ray excited at $x^{(3)}$ and recorded at $x^{(4)}$ or vice versa. Combining equations (4), (8), and (12), we find that the shear-wave slowness vectors at R [$\mathbf{p}^{S}(x^{(3)} \to R)$ and $\mathbf{p}^{S}(R \to x^{(4)})$] satisfy Snell's law:

$$\left[\mathbf{p}^{S}\left(x^{(3)} \to R\right) - \mathbf{p}^{S}\left(R \to x^{(4)}\right)\right] \times \mathbf{b}(R) = 0. \quad (13)$$

Therefore, the ray $x^{(3)}Rx^{(4)}$ corresponds to a pure SS reflection for the source and receiver positions at $x^{(3)}$ and $x^{(4)}$. As follows
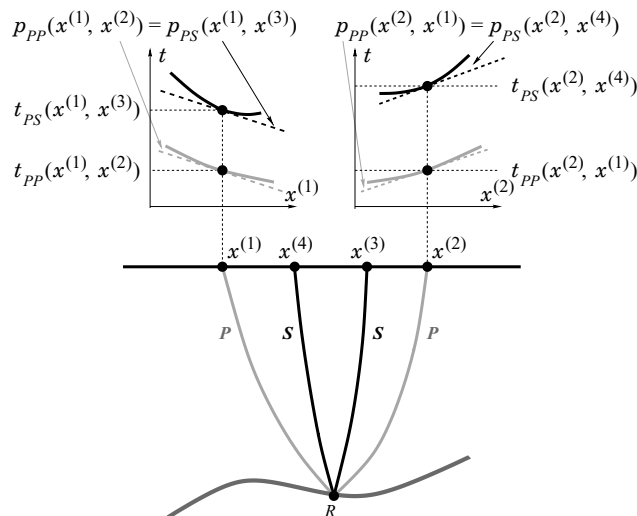

FIG. 3. Matching the reflection slopes on common-receiver PP and PS sections at locations $x^{(1)}$ and $x^{(2)}$ helps to find the source–receiver coordinates $x^{(3)}$ and $x^{(4)}$ of the pure SS ray $x^{(3)}Rx^{(4)}$. This reconstructed SS ray has the same reflection point R as the PP ray $x^{(1)}Rx^{(2)}$ and PS rays $x^{(1)}Rx^{(3)}$ and $x^{(2)}Rx^{(4)}$.

from Figure 3, the reflection traveltime $t_{SS}(x^{(3)}, x^{(4)})$ along this ray is given by

$$t_{SS}\left(x^{(3)}, x^{(4)}\right) = t_{PS}\left(x^{(1)}, x^{(3)}\right) + t_{PS}\left(x^{(2)}, x^{(4)}\right) \\ - t_{PP}\left(x^{(1)}, x^{(2)}\right). \quad (14)$$

Hence, the traveltime of the pure SS reflection is found as a simple combination of the measured PP and PS traveltimes. The receiver positions $x^{(3)}$ and $x^{(4)}$ for the PS arrivals are inferred from the slopes on common-receiver PP and PS gathers without using any information about the subsurface velocity model.

Extension to 3-D

The simplicity of our methodology can be maintained for 3-D multiazimuth multicomponent data. Let us assume that the sources and receivers cover a certain area in the acquisition plane $\mathbf{x} = [x_1, x_2]$. Then, for a given P-wave receiver $\mathbf{x}^{(2)} = [x_1^{(2)}, x_2^{(2)}]$ we build a common-receiver gather (data cube) in the vicinity of the source $\mathbf{x}^{(1)} = [x_1^{(1)}, x_2^{(1)}]$. The PP-wave reflection slope

$$\mathbf{p}_{PP}\left(\mathbf{x}^{(1)}, \mathbf{x}^{(2)}\right) = \left. \frac{dt_{PP}\left(\mathbf{x}, \mathbf{x}^{(2)}\right)}{d\mathbf{x}} \right|_{\mathbf{x}=\mathbf{x}^{(1)}} \quad (15)$$

and the traveltime $t_{PP}\left(\mathbf{x}^{(1)}, \mathbf{x}^{(2)}\right)$ are found by tracking the event inside the 3-D data volume corresponding to the receiver located at $\mathbf{x}^{(2)}$. The two-component vector $\mathbf{p}_{PP} = [p_{PP,1}, p_{PP,2}]$, which is equal to the horizontal projection of the traveltime gradient, can be found either by fitting a plane to the traveltime surface $t_{PP}([x_1, x_2], \mathbf{x}^{(2)})$ or by numerical differentiation of the obtained traveltime table t_{PP}.

Similarly, we obtain the local reflection slope of the PS-wave excited at $\mathbf{x}^{(1)}$ and recorded at $\mathbf{x}^{(3)}$,

$$\mathbf{p}_{PS}\left(\mathbf{x}^{(1)}, \mathbf{x}^{(3)}\right) = \left. \frac{dt_{PS}\left(\mathbf{x}, \mathbf{x}^{(3)}\right)}{d\mathbf{x}} \right|_{\mathbf{x}=\mathbf{x}^{(1)}}, \quad (16)$$

and the corresponding traveltime $t_{PS}\left(\mathbf{x}^{(1)}, \mathbf{x}^{(3)}\right)$. If the coordinates $\mathbf{x}^{(3)} = [x_1^{(3)}, x_2^{(3)}]$ of the PS-wave receiver satisfy the condition

$$p_{PP,i}\left(\mathbf{x}^{(1)}, \mathbf{x}^{(2)}\right) = p_{PS,i}\left(\mathbf{x}^{(1)}, \mathbf{x}^{(3)}\right), \quad (i = 1, 2) \quad (17)$$

for both horizontal components of the vectors $\mathbf{p}_{PP}$ and $\mathbf{p}_{PS}$, the PP and PS rays have the same reflection point R.

Next, switching the P-wave source and receiver positions exactly as has been done in two dimensions, we find the coordinates $\mathbf{x}^{(4)} = [x_1^{(4)}, x_2^{(4)}]$ of the second PS-wave receiver and the corresponding traveltime $t_{PS}(\mathbf{x}^{(2)}, \mathbf{x}^{(4)})$. Finally, the pure shear-wave traveltime $t_{SS}(\mathbf{x}^{(3)}, \mathbf{x}^{(4)})$ is obtained from equation (14).

NUMERICAL TEST

To demonstrate the performance of the above method, we present a numerical test using reflection traveltimes computed by anisotropic ray tracing (e.g., Gajewski and Pšenčík, 1987). Although such a test can be generated for 3-D heterogeneous anisotropic media, we restrict ourselves to a 2-D example for a VTI model composed of homogeneous layers (Figure 4).

The irregular (curved) interfaces in the overburden were introduced to create lateral heterogeneity.

We traced the rays corresponding to the PP and PSV reflections from the bottom of the model between 21 sources and 21 receivers with the coordinates $x = i \, \Delta x$, $\Delta x = 0.1$ km, $i = 0, \ldots, 20$ (Figure 4 shows the rays recorded at $x = 0.5$ km). The contours of the reflection traveltimes t_{PP} and t_{PS} for all computed rays are plotted in Figure 5. Note that while the PP-wave traveltimes (Figure 5a) are symmetric with respect to zero offset in accordance with equation (1), the converted-wave times (Figure 5b) are not. The asymmetry of the PS-wave moveout, however, does not impede our algorithm designed to generate the corresponding pure SS traveltimes.

The ray-traced traveltime tables t_{PP} and t_{PS} (each contains $21 \cdot 21 = 441$ values) represent the input data needed to reconstruct the shear-wave traveltimes t_{SS}. First, the reflection slopes on common-receiver gathers were computed by simple two-point linear interpolation. The approximation for the slope $p_{PP}(x^{(1)}, x^{(2)})$ [equation (??)], for example, is

$$p_{PP}\left(x^{(1)}, x^{(2)}\right)$$
$$\approx \frac{t_{PP}\left(x^{(1)} + \Delta x, \, x^{(2)}\right) - t_{PP}\left(x^{(1)} - \Delta x, \, x^{(2)}\right)}{2\Delta x}. \quad (18)$$

For each pair $(x^{(1)}, x^{(2)})$, we find the coordinates of the corresponding SS-wave sources and receivers $x^{(3)}$ and $x^{(4)}$ (Figure 6)

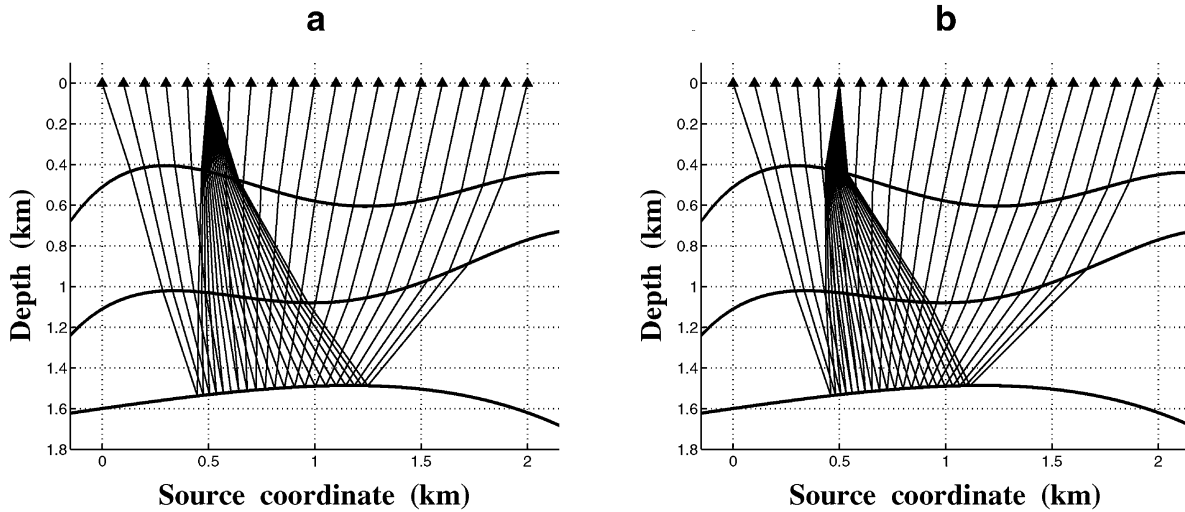**a**   **b**

FIG. 4. Reflected (a) PP and (b) PSV rays recorded by the receiver at $x = 0.5$ km in a 2-D model containing three homogeneous VTI layers separated by irregular interfaces. The vertical velocities in the layers (from top to bottom) are $V_{P0,1} = 2.0$ km/s, $V_{S0,1} = 0.8$ km/s; $V_{P0,2} = 2.5$ km/s, $V_{S0,2} = 1.25$ km/s; and $V_{P0,3} = 3.0$ km/s, $V_{S0,3} = 1.8$ km/s. Thomsen (1986) anisotropic parameters are $\epsilon_1 = 0.20$, $\delta_1 = 0.10$; $\epsilon_2 = 0.25$, $\delta_2 = 0.05$; and $\epsilon_3 = 0.15$, $\delta_3 = 0.10$.
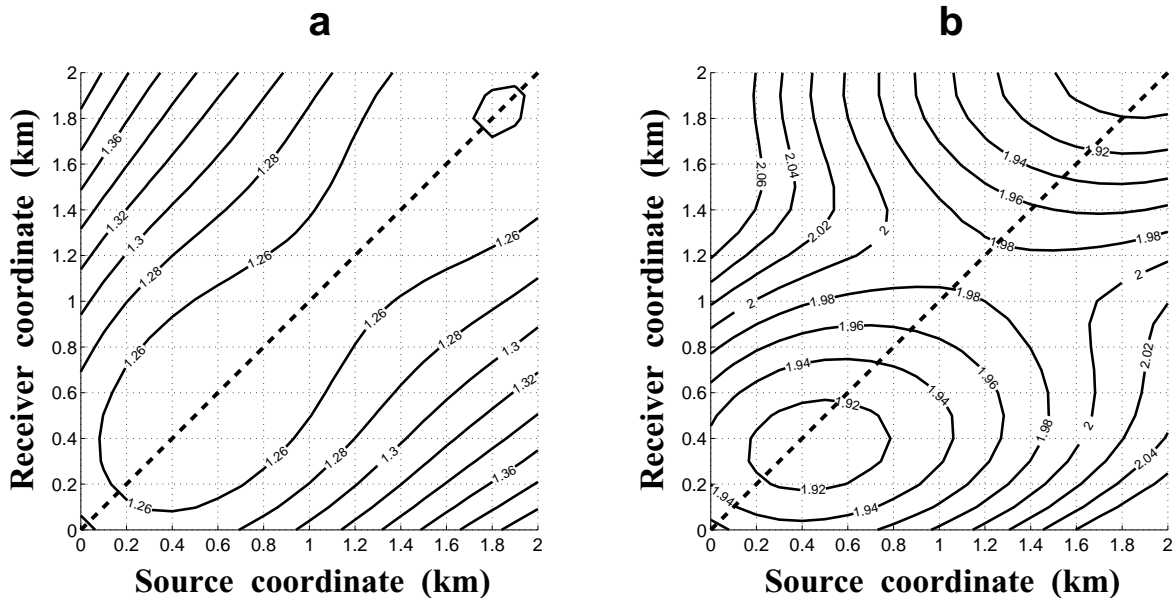
a   **b**

FIG. 5. Traveltime contours (a) t_{PP} and (b) t_{PS} for the model shown in Figure 4. The dashed lines indicate the zero-offset (a) PP and (b) PS reflections.

by matching the slopes of PP and PS arrivals on common-receiver gathers as described above [equations (6) and (11)]. Since $x^{(3)}$ and $x^{(4)}$ do not necessarily coincide with the source–receiver locations used in the modeling, we applied linear interpolation between the slopes on adjacent common-receiver gathers. The source and receiver positions for the pure SS arrivals in Figure 6 are symmetric with respect to the zero-offset line (dashed) because of reciprocity.

Note the absence of the reconstructed SS-wave sources and receivers for relatively large offsets (the lower right and upper left corners in Figure 6). Since the P-to-S velocity ratio is always greater than unity ($V_P > V_S$), the reconstructed SS rays are closer to the reflector normal than are the corresponding PP rays, as schematically shown in Figure 3. Therefore, in the absence of strong lateral heterogeneity in the overburden, the source–receiver distance (offset) for the obtained SS reflections is generally smaller than the offsets for the recorded PP- and PS-waves; this is confirmed by Figure 6.

The relationship between the offsets of PP- and SS-waves can be estimated from the approximation of Tessmer and Behle (1988) derived for a single isotropic homogeneous layer above a horizontal reflector:

$$h_{SS} \approx \frac{2}{1+\gamma} h_{PS} \approx \frac{1}{\gamma} h_{PP}, \qquad (19)$$

where h_{SS}, h_{PS}, and h_{PP} are the offsets corresponding to the SS-, PS-, and PP-waves (respectively) and

$$\gamma \equiv \frac{V_P}{V_S}. \qquad (20)$$

For a typical value $\gamma = 2$, approximations (19) yield

$$h_{SS} \approx \frac{2}{3} h_{PS} \approx \frac{1}{2} h_{PP}, \qquad (21)$$

which is reasonably close to the result in Figure 6.

Another interesting observation is that Figure 6 contains only 417 reconstructed positions of SS-wave sources and receivers, whereas the number of PP (and PS) data points is 441.
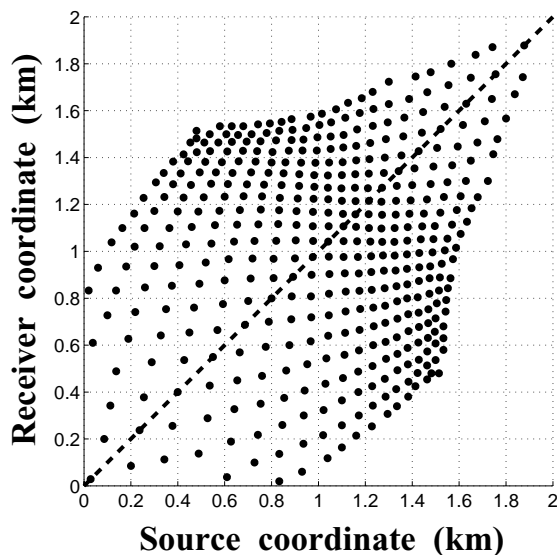
This happens because the curved intermediate interfaces in our model (Figure 4) produce PP reflection slopes on some common-receiver gathers that cannot be matched with any measured PS-wave slopes. Figure 7 gives an example of such a situation for the source located at 0.1 km. Clearly, the PP slopes p_{PP} for the receivers at 0.0 and 0.1 km are greater than any of the available PS slopes. This means that the PS-wave receiver locations $x^{(3)}$ sought by our algorithm are outside of our source–receiver array, and no SS traveltime can be reconstructed for the PP-wave source–receiver pairs ($x^{(1)} = 0.1$ km, $x^{(2)} = 0.0$ km) and ($x^{(1)} = 0.1$ km, $x^{(2)} = 0.1$ km). However, as shown below, the absence of SS reflections for some source–receiver pairs does not compromise the quality of the reconstructed traveltimes t_{SS} elsewhere.

To verify the accuracy of our method, the SS-wave traveltimes obtained from PP and SS data can be compared with those computed by ray tracing. The ray-traced traveltimes of the pure SS reflections for all 441 sources and receivers are shown in Figure 8. The contours of t_{SS} are symmetric with respect to the zero-offset line (dashed), as should be the case for pure-mode reflections [equation (1)]. The comparison in Figure 9 demonstrates that the traveltimes t_{SS} produced by our algorithm practically coincide with the ray-traced values within the area occupied by the reconstructed SS-wave sources and receivers in Figure 6. The maximum difference between the estimated and ray-traced traveltimes t_{SS} in Figure 9 is 1.6 ms. This error stems primarily from the linear approximation (18) for the reflection slopes and is enhanced by interpolating the PS-wave slopes in the process of searching for the receiver positions $x^{(3)}$ and $x^{(4)}$. An additional error is caused by interpolating the SS traveltimes (via 2-D smoothing polynomials) from the irregular grid in Figure 6 to the regular one used in the ray tracing.

Thus, PP and PS traveltimes (Figure 5) are sufficient for reconstructing the corresponding SS-wave traveltimes (Figure 8). It should be emphasized that as long as both PP- and PS-waves are reflected from the same interface, our method is exact, with errors caused solely by traveltime picking and numerical implementation.
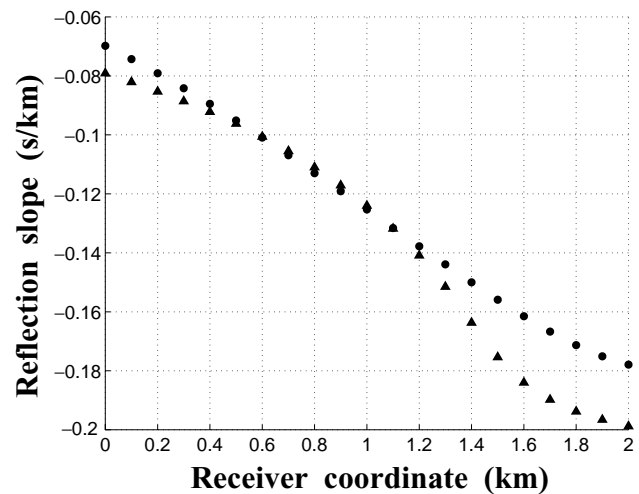
FIG. 6. Coordinates of the SS-wave sources-receiver pairs reconstructed from the PP and PS data for the test in Figure 4.

FIG. 7. Reflection slopes p_{PP} (dots) and p_{PS} (triangles) at the source location computed by ray tracing for the source at 0.1 km.
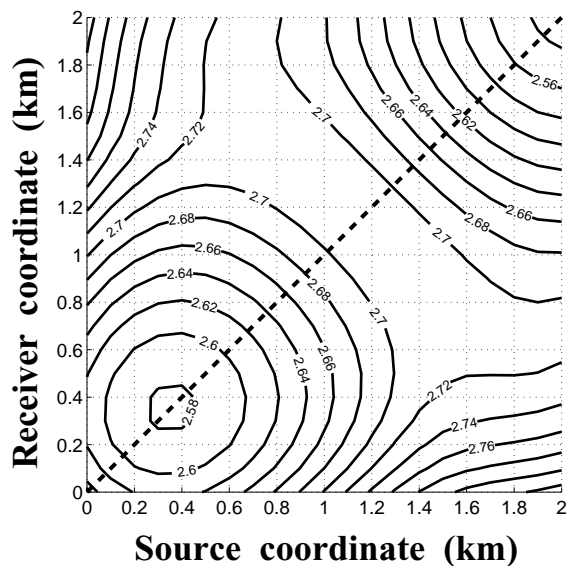
DISCUSSION

Although the numerical example above was given for a 2-D line, we have also successfully tested the methodology on 3-D multiazimuth, multicomponent synthetic data. The only reason for not showing those results here is the difficulty of displaying 4-D traveltime fields, such as $t_{PP}([x_1^{(1)}, x_2^{(1)}], [x_1^{(2)}, x_2^{(2)}])$, and 4-D cubes of the reconstructed SS-wave source and receiver positions $(\mathbf{x}^{(3)}, \mathbf{x}^{(4)}) = ([x_1^{(3)}, x_2^{(3)}], [x_1^{(4)}, x_2^{(4)}])$.

The numerical test was performed under ideal, noise-free conditions and yielded almost perfect results. Since field-data application may be hampered by such factors as noise, missing data, and errors in interpretation, their influence is examined below.

Influence of noise

To simulate traveltime picking errors, we added Gaussian noise with a standard deviation of 2 ms to the input data (the PP and PS traveltimes in Figure 5) and repeated the whole procedure. Figure 10 shows that the reconstructed positions of the SS-wave sources and receivers are substantially different from those in Figure 6. These errors were produced by equation (18), which represents the simplest finite-difference approximation
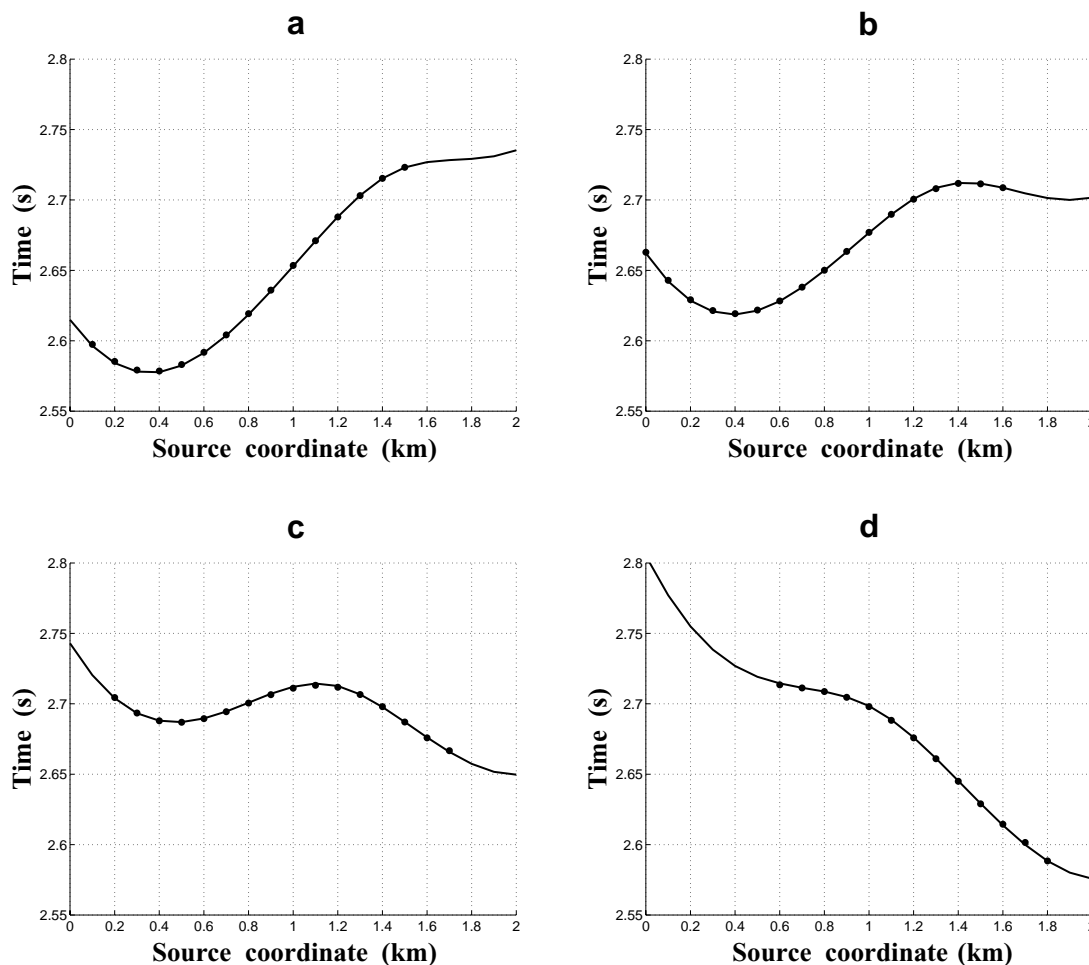

FIG. 8. Contours of the ray-traced SS-wave traveltimes t_{SS}.

FIG. 9. Comparison of the ray-traced (solid lines) and reconstructed (dots) traveltimes t_{SS} for the receivers located at (a) 0.4, (b) 0.8, (c) 1.2, and (d) 1.6 km.
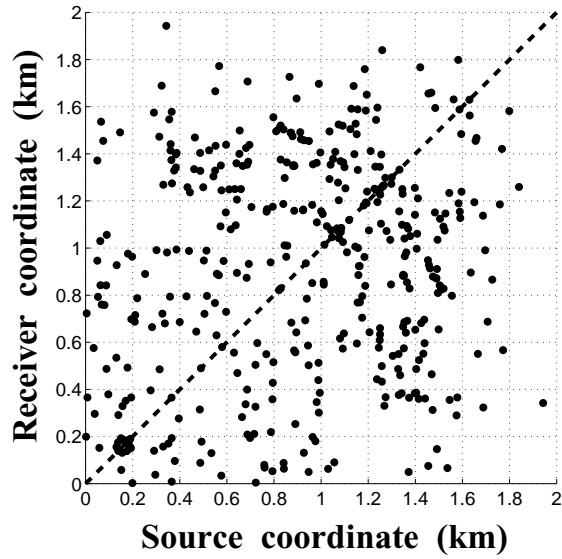
FIG. 10. Same as Figure 6 but after adding Gaussian noise with a standard deviation of 2 ms to the input PP and PS traveltimes.

of the derivative $dt_{PP}(x, x^{(2)})/dx$ and thus amplifies random errors in the traveltimes.

To reduce the instability in the slope estimates, one should compute them by fitting straight lines to several data points (not to just two as was done here) or employ quadratic polynomials. In our example, however, some additional smoothing was provided by the polynomials used to interpolate and regrid the reconstructed traveltimes t_{SS}. As a result, the SS traveltimes in Figure 11 show less scatter than that in the source and receiver positions in Figure 10, with the maximum deviation from the ray-traced traveltimes t_{SS} reaching 9 ms. The largest errors concentrate near the edges of the area covered by the reconstructed positions of the SS-wave sources and receivers (compare Figure 10 with Figures 11a and 11b). Clearly, those edge distortions can be removed by reducing the size of this area used for further processing of the SS data.

Small PS reflection coefficient

Another potential problem for our method may be caused by the small amplitude and the associated polarity reversal of converted waves. It is known that the PS-wave reflection coefficient for gently dipping reflectors often vanishes in some vicinity of zero offset. [The words "some vicinity" refer to the
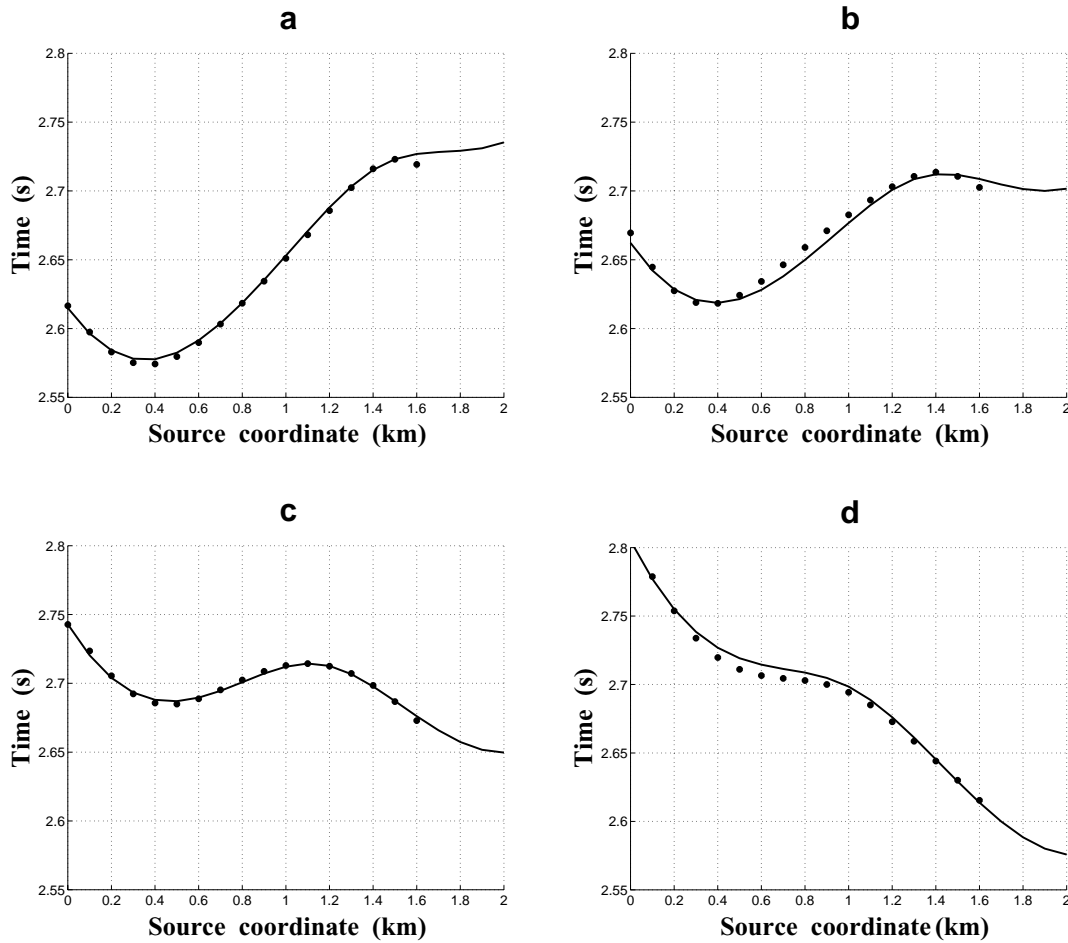

FIG. 11. Same as Figure 9 but after adding the noise to the data.

fact that the PS-wave reflection coefficient does not necessarily vanish at zero offset if the medium immediately above or below the reflector is anisotropic. In fact, for reflector dips beyond 30°, the amplitude of the PS-wave in VTI media goes to zero at relatively large source–receiver offsets (Tsvankin and Grechka, 2000a)]. This leads to a polarity reversal and a reduction in the PS-wave amplitude for a certain range of offsets. To model the implications of this phenomenon in the reconstruction of the SS traveltimes, we muted out the stripe of the PS traveltime data (Figure 5b) with offsets $h_{PS} < 0.4$ km, assuming that the traveltimes t_{PS} at small offsets cannot be picked in a reliable way because of the small reflection amplitude.

Repeating the procedure described above, we found the positions of SS-wave sources and receivers shown in Figure 12. Comparison of this plot with Figure 6 reveals the absence of reconstructed SS data at small source–receiver offsets. Also, the number of obtained data points is down to 269 from 417 in Figure 6.

The missing data, however, do not prevent our method from accurately reconstructing the traveltimes t_{SS} in other areas (compare Figure 13 with Figure 9). The gaps in Figure 13 correspond to the missing data where the traveltimes t_{SS} (dots) could have been found only by interpolation and extrapolation.

The results in Figures 12 and 13 can be explained by the locality of the slope estimates in our method. Indeed, since the traveltimes t_{SS} are obtained from local measurements of the traveltimes t_{PP}, t_{PS} and their slopes, the absence of PS data for a certain range of offsets does not adversely influence the performance of our procedure for other offsets.

Interpretation errors

An important assumption of our method is that the PP- and PS-waves are reflected from the same interface in the subsurface. Correlation of PP and PS reflections, however, is not straightforward and often requires additional information, such as borehole data. Possible consequences of interpretation errors in correlating PP and PS data are illustrated in Figure 14.
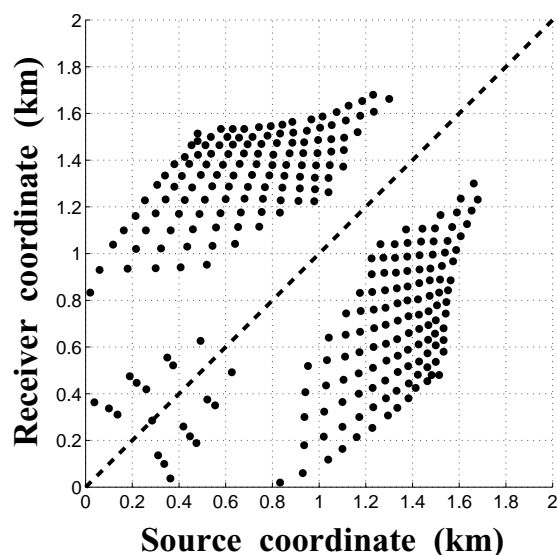

FIG. 12. Same as Figure 6 but after muting out the PS traveltimes for offsets $h_{PS} < 0.4$ km.

If the PS event is reflected from a deeper interface than the PP reflection (Figure 14a), our method will reconstruct the trajectory $x^{(4)} R_1 R R_2 x^{(3)}$ corresponding to a peg-leg multiple SPPS with two PS conversions at points R_1 and R_2. Equation (14) in this case yields

$$t_{SS} = t_{x^{(4)}R_1} + t_{R_1R} + t_{RR_2} + t_{R_2 x^{(3)}}, \qquad (22)$$

where $t_{x^{(4)}R_1}, t_{R_1R}, t_{RR_2}$, and $t_{R_2 x^{(3)}}$ are the traveltimes along the ray segments shown in Figure 14a (t_{R_1R} and t_{RR_2} actually correspond to the P-wave). The traveltime in equation (22) clearly differs from the traveltime of the SS-wave primary reflection from either of the two interfaces.

In contrast, if the PS-wave is reflected from a more shallow interface than the PP-wave (Figure 14b), the reconstructed traveltime does not correspond to any physical ray. Applying equation (14), we obtain

$$t_{SS} = t_{x^{(4)}R_1} - t_{R_1R} - t_{RR_2} + t_{R_2 x^{(3)}}, \qquad (23)$$

where t_{R_1R} and t_{RR_2} are P-wave traveltimes. The value of t_{SS} in equation (23) can even become negative if the two interfaces in Figure 14b are sufficiently separated in depth.

Thus, any errors in identifying and correlating PP- and PS-reflections inevitably lead to incorrect traveltimes t_{SS}. The difference in the kinematics of the correct and erroneously reconstructed events (in particular, the difference between their stacking velocities), however, might provide a criterion that can be used to avoid interpretation errors.

CONCLUSIONS

We have suggested a method for reconstructing the traveltimes of pure SS-wave primaries from PP- and PS-wave reflection data. The key element of our approach is matching the reflection slopes on common-receiver sections to identify PP- and PS-waves reflected at the same (but generally unknown) subsurface points. The algorithm can be implemented in either two or three dimensions by tracking the PP and PS events inside the prestack data volumes. The main features of the method are summarized below.

1) The method is based on the sole assumption that the data (PP-wave and PS-wave primary reflections) correspond to the same reflector. Note that correlation of PP and PS traveltimes requires some knowledge about the model and may be rather complicated in practice. Other than that, the method is entirely data driven, and no information about the subsurface velocity field is needed.

2) The method operates with local reflection slopes (horizontal slownesses) on common-receiver sections. This locality helps to avoid a number of complications inherent in processing of converted-wave data, such as

   a) *Asymmetry of PS traveltimes and the diodic nature of PS-wave NMO velocity.*—Since the algorithm needs only local reflection slopes on common-receiver gathers, the asymmetry of PS moveout is irrelevant.

   b) *Reflection-point dispersal for converted waves.*—PS-wave CMP gathers, which suffer from reflection-point dispersal, are not used in the computation

of SS traveltimes. The reflection points of the PS-waves and the reconstructed SS-waves are guaranteed to be exactly the same as those for the corresponding PP-waves. (The actual locations of the reflection points, however, remain unknown prior to velocity analysis.) The reflection-point dispersal on the reconstructed SS-wave CMP gathers is much smaller than that on PS-wave gathers.
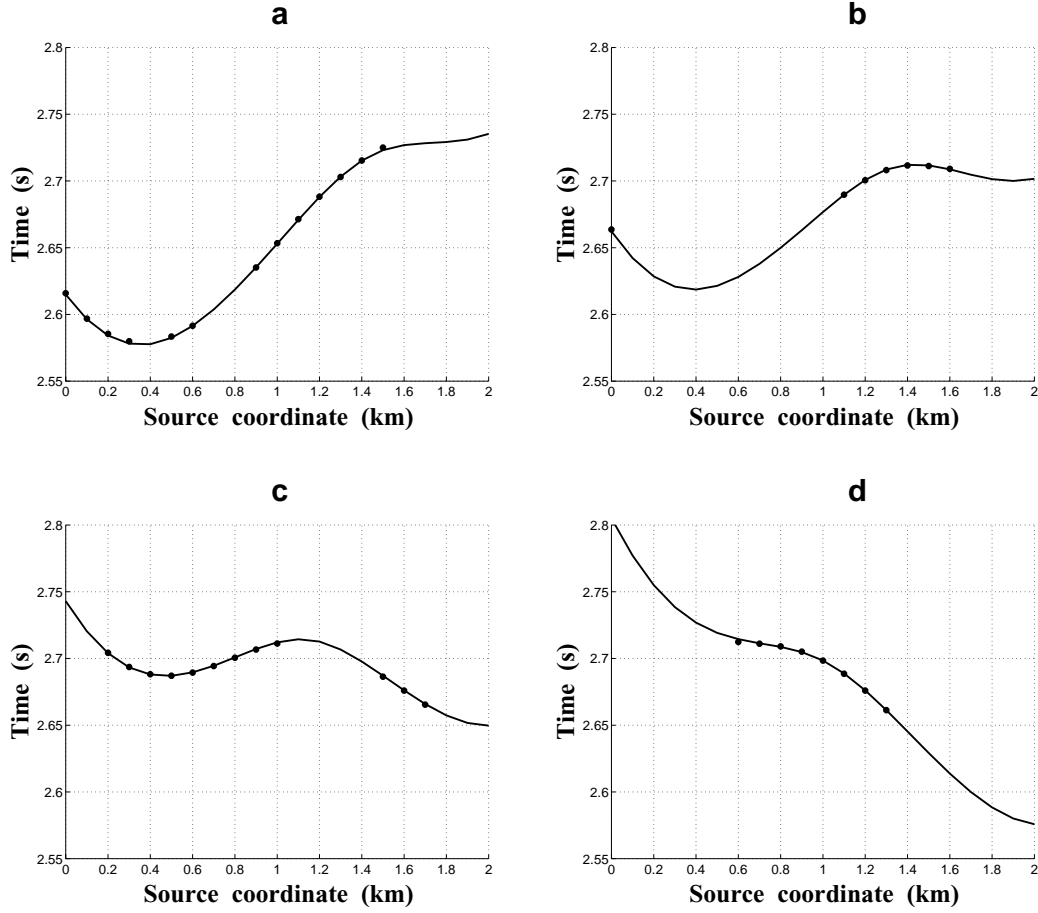

FIG. 13. Same as Figure 9 but after muting out the PS traveltimes for offsets $h_{PS} < 0.4$ km.
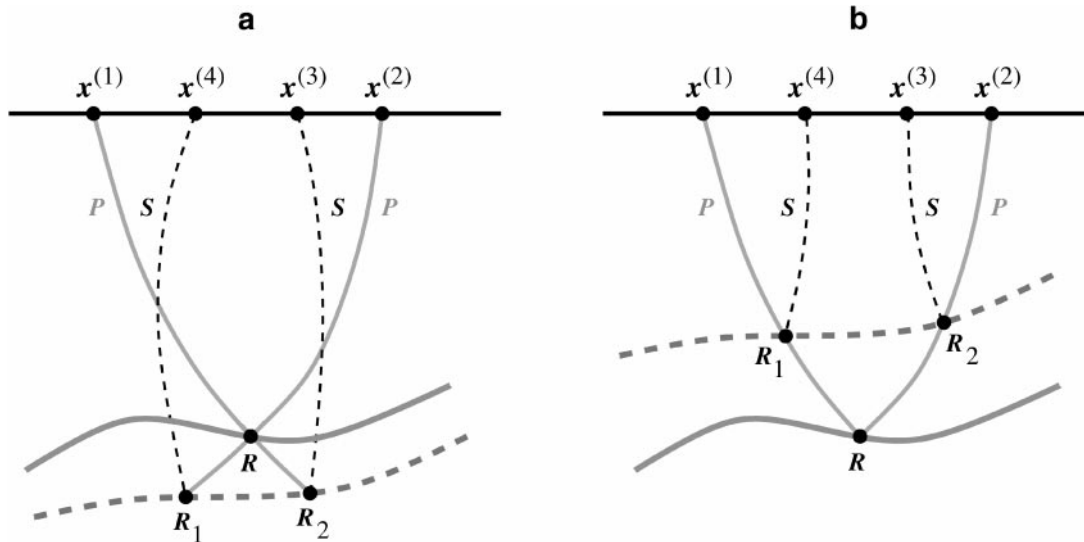

FIG. 14. If the PP- and PS-waves are reflected from different interfaces, our method will produce the SS traveltimes corresponding to either (a) a peg-leg multiple or (b) a nonexistent raypath.

c) *Polarity reversal.*—Small amplitudes of PS-waves in the vicinity of the polarity reversal hamper traveltime picking in those areas. The locality of our method makes it possible to mute out low-amplitude PS traces without compromising the quality of results obtained from the remaining data.

3) The SS traveltimes t_{SS} reconstructed by our method are exact. Provided the PP- and PS-wave are reflected from the same interface, t_{SS} may be distorted only by errors in the estimation of the reflection slopes and interpolation or extrapolation of the slopes and traveltimes.

4) Once the traveltimes t_{SS} are found, they can be processed by means of any velocity-analysis technique developed for pure modes. The reconstructed SS-wave moveout velocities are especially attractive for anisotropic stacking-velocity tomography because they provide information complementary to that in PP-wave data (Grechka, Pech, and Tsvankin, 2001).

5) To ensure that the SS data are reconstructed for a sufficiently wide range of source–receiver offsets, it is necessary to use long-offset input PP data. For the offset-to-depth ratio of the SS-waves to be close to unity (the value required for stable moveout velocity analysis), the maximum offset of the PP-waves should reach or exceed (depending on the P-to-S velocity ratio) about twice the reflector depth.

6) While our method provides an accurate kinematic treatment of PP, PS, and SS wavefields for models of arbitrary complexity, it is not amplitude preserving and is not designed to recover the correct amplitudes of SS reflections.

Application of the method to multicomponent 2-D field data is described by Grechka, Tsvankin, et al. (2001).

ACKNOWLEDGMENTS

REFERENCES

Alkhalifah, T., and Tsvankin, I., 1995, Velocity analysis for transversely isotropic media: Geophysics, **60**, 1550–1566.

Gaiser, J. E., 2000, Advantages of 3-D PS-wave data to unravel S-wave birefringence for fracture detection: 70th Ann. Internat. Mtg., Soc. Expl. Geophys., Expanded Abstracts, 1201–1204.

Gajewski, D., and Pšenčík, I., 1987, Computation of high frequency seismic wavefields in 3-D laterally inhomogeneous anisotropic media: Geophys. J. Roy. Astr. Soc., **91**, 383–412.

Granli, J. R., Arntsen, B., Sollid, A., and Hilde, E., 1999, Imaging through gas-filled sediments using marine shear-wave data: Geophysics, **64**, 668–677.

Grechka, V., and Tsvankin, I., 1998, 3-D description of normal moveout in anisotropic inhomogeneous media: Geophysics, **63**, 1079–1092.

Grechka, V., Contreras, P., and Tsvankin, I., 2000, Inversion of normal moveout for monoclinic media: Geophys. Prosp., **48**, 577–602.

Grechka, V., Pech, A., and Tsvankin, I., 2000a, Inversion of P-wave data in laterally heterogeneous VTI media—Part I: Plane dipping interfaces: 70th Ann. Internat. Mtg., Soc. Expl. Geophys., Expanded Abstracts, 2225–2228.

——— 2000b, Inversion of P-wave data in laterally heterogeneous VTI media—Part II: Irregular interfaces: 70th Ann. Internat. Mtg., Soc. Expl. Geophys., Expanded Abstracts, 2229–2232.

——— 2001, Multicomponent stacking-velocity tomography for transversely isotropic media: 71st Ann. Internat. Mtg., Soc. Expl. Geophys., Expanded Abstracts, 1847–1850.

Grechka, V., Theophanis, S., and Tsvankin, I., 1999, Joint inversion of P- and PS-waves in orthorhombic media: Theory and a physical-modeling study: Geophysics, **64**, 146–161.

Grechka, V., Tsvankin, I., Bakulin, A., and Hansen, J. O., 2001, Joint inversion of PP and PS reflection data for VTI media: A North Sea case study: 71st Ann. Internat. Mtg., Soc. Expl. Geophys., Expanded Abstracts, 2112–2115.

Pérez, M. A., Grechka, V., and Michelena, R. J., 1999, Fracture detection in a carbonate reservoir using a variety of seismic methods: Geophysics, **64**, 1266–1276.

Seriff, A. J., and Sriram, K. P., 1991, P-SV reflection moveouts for transversely isotropic media with a vertical symmetry axis: Geophysics, **56**, 1271–1274.

Tessmer, G., and Behle, A., 1988, Common reflection point data-stacking technique for converted waves: Geophys. Prosp., **36**, 671–688.

Thomsen, L., 1986, Weak elastic anisotropy: Geophysics, **51**, 1954–1966.

——— 1999, Converted-wave reflection seismology over inhomogeneous, anisotropic media: Geophysics, **64**, 678–690.

Tsvankin, I., and Grechka, V., 2000a, Dip moveout of converted waves and parameter estimation in transversely isotropic media: Geophys. Prosp., **48**, 257–292.

——— 2000b, Two approaches to anisotropic velocity analysis of converted waves: 70th Ann. Internat. Mtg., Soc. Expl. Geophys., Expanded Abstracts, 1193–1196.

Tsvankin, I., and Thomsen, L., 1994, Nonhyperbolic reflection moveout in anisotropic media: Geophysics, **59**, 1290–1304.